

Self-Bound Quantum Droplets of Atomic Mixtures in Free Space

G. Semeghini,^{1,2,*} G. Ferioli,^{1,2} L. Masi,^{1,2} C. Mazzinghi,¹ L. Wolswijk,¹ F. Minardi,^{2,1,3} M. Modugno,^{4,5}
G. Modugno,^{1,2} M. Inguscio,^{2,1} and M. Fattori^{1,2}

¹*LENS and Dipartimento di Fisica e Astronomia, Università di Firenze, 50019 Sesto Fiorentino, Italy*

²*CNR Istituto Nazionale Ottica, 50019 Sesto Fiorentino, Italy*

³*Dipartimento di Fisica e Astronomia, Università di Bologna, 40127 Bologna, Italy*

⁴*Departamento de Física Teórica e Historia de la Ciencia, Universidad del País Vasco UPV/EHU, 48080 Bilbao, Spain*

⁵*IKERBASQUE, Basque Foundation for Science, 48011 Bilbao, Spain*



(Received 25 October 2017; published 7 June 2018)

Self-bound quantum droplets are a newly discovered phase in the context of ultracold atoms. In this Letter, we report their experimental realization following the original proposal by Petrov [*Phys. Rev. Lett.* **115**, 155302 (2015)], using an attractive bosonic mixture. In this system, spherical droplets form due to the balance of competing attractive and repulsive forces, provided by the mean-field energy close to the collapse threshold and the first-order correction due to quantum fluctuations. Thanks to an optical levitating potential with negligible residual confinement, we observe self-bound droplets in free space, and we characterize the conditions for their formation as well as their size and composition. This work sets the stage for future studies on quantum droplets, from the measurement of their peculiar excitation spectrum to the exploration of their superfluid nature.

DOI: [10.1103/PhysRevLett.120.235301](https://doi.org/10.1103/PhysRevLett.120.235301)

Ultracold atoms are commonly known and studied in their gas phase. They are confined on a finite volume by external potentials, but they readily expand as they are released from their container. A recent theoretical proposal [1] has surprisingly pointed out that a Bose-Bose mixture of diluted weakly interacting atomic gases can form liquidlike droplets, which are self-bound in free space and whose equilibrium densities are independent of the atom number. When the attraction between the two atomic species becomes larger than the single-species average repulsion, the mixture is expected to collapse according to the mean-field (MF) theory [2]. In this regime, instead, an effective repulsion provided by the first beyond-mean-field correction to the energy, the so-called Lee-Huang-Yang (LHY) term [3], arises to arrest collapse and stabilize the system. The equilibrium between the two competing forces leads to the formation of a self-bound droplet, while the isotropic nature of the van der Waals interactions shapes its spherical geometry. This new quantum state of matter is expected to display a number of interesting features. The most peculiar among them is related to its excitation spectrum. In a specific region of the droplet phase diagram, the particle emission threshold is predicted to lie below any possible

excitation mode [1]. Any excess of energy is thus expelled by losing particles, leading to an effective self-evaporation and keeping the droplet at zero temperature.

The stabilization mechanism generated by the LHY correction has been recognized as responsible also for the formation of a different class of self-bound quantum systems, i.e., dipolar droplets [4–10]. While attractive mixtures create spherical droplets, in dipolar gases droplets are elongated along the dipole direction and, thus, strongly anisotropic. The different geometry, together with the different kinds of interactions governing the stabilization, leads to important differences in the properties of the two objects and enriches the range of phenomena that can be explored [11–13]. Recently, self-bound droplets have been observed also in bosonic mixtures, however, only in confined geometries [14,15]. These experiments confirmed the prediction of a liquidlike phase in attractive mixtures, but they also found some deviations from the theory [14–17]. The experimental investigation of mixture droplets in free space is then of primary interest, since it allows a direct verification of the model in Ref. [1] and it paves the way to studying the unique properties of spherical droplets. The phenomenon of self-evaporation is indeed predicted to vanish in the presence of a strong anisotropy, as in the dipolar case [18] or in strongly confined mixture droplets.

In this Letter, we study experimentally the formation of quantum droplets in a homonuclear bosonic mixture in free space. Exploiting magnetic Feshbach resonances, we tune the interatomic scattering lengths to reach the interaction regime where the mixture is predicted to be self-bound. We

Published by the American Physical Society under the terms of the [Creative Commons Attribution 4.0 International license](https://creativecommons.org/licenses/by/4.0/). Further distribution of this work must maintain attribution to the author(s) and the published article's title, journal citation, and DOI.

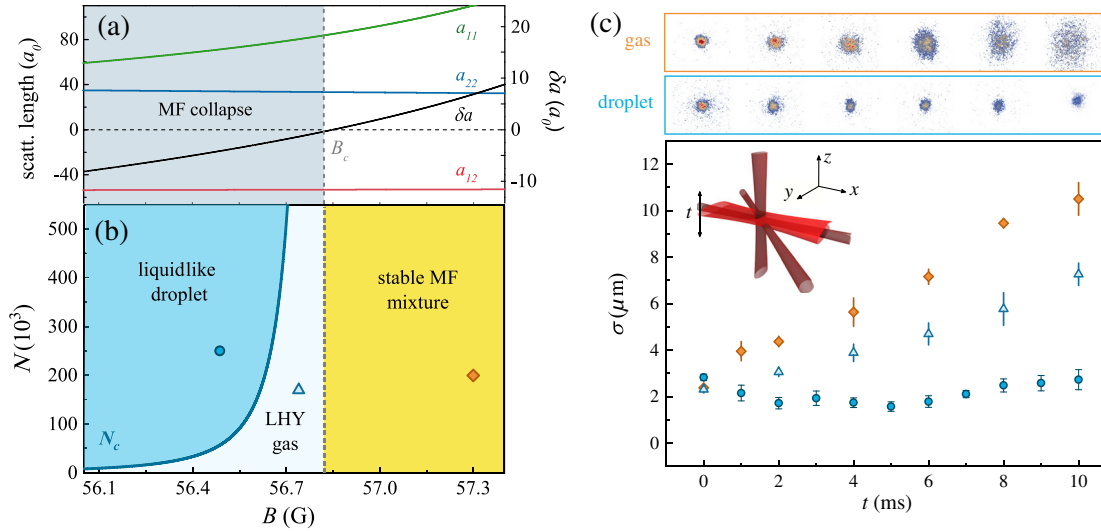


FIG. 1. (a) Intra- and interspecies scattering lengths between the hyperfine states $|1, 0\rangle$ (state 1) and $|1, -1\rangle$ (state 2) of ^{39}K , tuned by an external magnetic field B via Feshbach resonances. The resulting MF energy of the mixture is proportional to the effective scattering length δa , which becomes negative at $B_c = 56.85$ G. (b) Phase diagram for the mixture as a function of the atom number N and of the magnetic field B . (c) Evolution of the cloud in free space for three different points of the phase diagram in (b). The upper rows show the difference between the evolution of the density profiles in the gas and droplet phases. Inset: Schematic representation of the geometry of the experiment.

implement an optical levitating potential with negligible residual confinement along all directions, which allows us to have long interrogation times and access the droplet properties in free space. We probe the mixture phase diagram, proving the existence of a self-bound phase and identifying the critical conditions for its formation. We analyze the dynamics observed in the droplet formation and evolution and compare it to numerical simulations. We finally measure the droplet size and composition as a function of the attractive MF interaction, and we find a good agreement with the predictions from Ref. [1].

We create self-bound droplets using two hyperfine states of ^{39}K , namely, $|F = 1, m_F = 0\rangle$ (state 1) and $|F = 1, m_F = -1\rangle$ (state 2). Feshbach resonances allow us to tune the mutual contact interactions as represented in Fig. 1(a) as a function of the magnetic field B [19]. The intraspecies scattering lengths a_{11} and a_{22} are both positive, while the interspecies a_{12} is negative. We define an effective scattering length for the mixture $\delta a = a_{12} + \sqrt{a_{11}a_{22}}$, which becomes negative for $B < B_c$, setting the threshold for collapse in the usual MF picture [2]. The stabilization effect of the LHY correction predicted in Ref. [1] appears exactly here. Contrary to the case of a single species [20], in a mixture of Bose-Einstein condensates (BECs) the MF and LHY terms have a different dependence on the interparticle scattering lengths. While the MF energy E_{MF} is proportional to $|\delta a|$ and thus vanishes close to B_c , the LHY correction E_{LHY} scales with a_{11} and a_{22} [21], thus becoming comparable to the MF term in this regime. Moreover, the two terms have a different dependence on the density n , since $E_{\text{MF}} \propto n^2$ while $E_{\text{LHY}} \propto n^{5/2}$. This means that, when the MF contribution becomes negative, leading to an uncontrolled

increase of density and eventually to collapse, the positive LHY term, having a steeper dependence on n , arrests the collapse and stabilizes the system. In this regime, the mixture can be found in two different phases depending on the total atom number N . When N is larger than a critical number N_c , the mixture forms a self-bound liquidlike droplet [1,29]. Below that threshold, the kinetic energy overcomes the MF attraction, and the system goes back into an expanding gas phase, labeled as LHY gas in the phase diagram in Fig. 1(b).

We prepare a BEC of ^{39}K atoms in state 2, in a crossed dipole trap, created by three red-detuned laser beams, with trapping frequencies $\omega_x = 2\pi \times 195(10)$ Hz, $\omega_y = 2\pi \times 180(10)$ Hz, and $\omega_z = 2\pi \times 220(10)$ Hz, along the axes sketched in Fig. 1(c). A homogeneous magnetic field B is used to tune the scattering lengths as in Fig. 1(a). Starting with a BEC with up to 4×10^5 atoms, we ramp linearly B in 20 ms to a desired target value, and then we apply a radio-frequency (rf) pulse of $10 \mu\text{s}$ to transfer $\sim 50\%$ of the atoms in state 1. In order to observe the subsequent evolution for sufficiently long times, remaining within the field of view of our imaging system, gravity compensation is required. The vertical position of a red-detuned elliptical laser beam is modulated in time with an acousto-optical modulator at a frequency of 4 kHz, such that the averaged potential experienced by the atoms provides a gradient opposite to gravity [red beam in the inset in Fig. 1(c)]. A large waist on the horizontal direction (y) and a suitable time modulation along the vertical direction (z) guarantee negligible residual curvatures on all directions [21]. At the end of the rf pulse, we switch off the dipole traps and switch on the levitating

potential to observe the expansion of the mixture. After a variable waiting time, we record the density profile of the cloud via absorption imaging along the y direction, with optical resolution $\delta_{\text{res}} = 0.8_{-0.2}^{+0.1} \mu\text{m}$ [21]. We fit it with a two-dimensional Gaussian and measure the size along x and z as the half-width at $1/\sqrt{e}$. In order to probe the different phases expected for the mixture, we study the expansion of the cloud in three different points of the phase diagram in Fig. 1(b). In Fig. 1(c), we report the average size $\sigma = \sqrt{\sigma_x \sigma_z}$ as a function of time t . The mixtures prepared with $\delta a > 0$ (orange diamonds) or $\delta a < 0$ and $N < N_c$ (light blue triangles) show the typical gas behavior: When released from the dipole trap, they expand at a finite velocity. For $\delta a < 0$ and $N > N_c$ (blue circles), instead, the size of the cloud remains essentially constant, proving the formation of a self-bound droplet.

To characterize the droplet phase, we also perform measurements of the total atom number and of the relative population in states 1 and 2. After a variable time, we perform a Stern-Gerlach separation of the two components, by

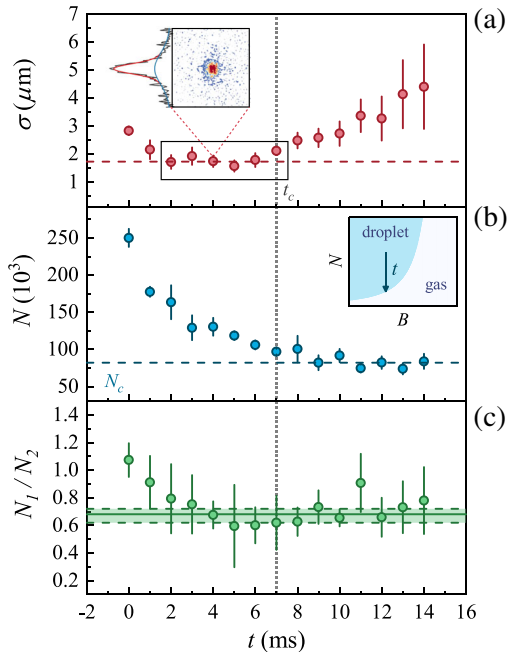


FIG. 2. Time evolution of σ (a), N (b), and N_1/N_2 (c) in the droplet phase at $B = 56.54(1)$ G. The inset in (a) reports the density profile of the droplet after some expansion time, together with the fitted bimodal function described in the text. In the inset in (b), we draw a sketch of the trajectory followed by the system in the mixture phase diagram during the time evolution, due to losses. The dashed line in (a) is the average of σ on the plateau identified by the rectangle. The dashed line in (b) is the critical atom number N_c , measured as the average of N for $t > t_c$. In (c), the solid line represents the theoretical equilibrium value $N_1/N_2 = \sqrt{a_{22}/a_{11}}$, and the green area between the dashed lines includes the allowed deviations $\delta N_i/N_i$ (see the text). The error bars represent the statistical uncertainty and correspond to one standard deviation.

applying a magnetic field gradient along the vertical direction z , so that we can count separately N_1 and N_2 . In Fig. 2, we report the evolution of the size σ , measured as in Fig. 1(c), of the total atom number $N = N_1 + N_2$ and of the ratio N_1/N_2 , for $B = 56.54(1)$ G. The data in Fig. 2(a) show that the mixture is in the self-bound regime only up to a critical time t_c , while afterwards it expands as a gas. This behavior can be understood by looking at $N(t)$ in Fig. 2(b). The atom number drops quite rapidly in the first 7 ms, so that the system follows the phase-diagram trajectory sketched in the inset in Fig. 2(b): At a given time, the atom number reaches N_c , and the system undergoes a droplet-to-gas transition, where the cloud starts to expand and the atom number stabilizes to a constant value. In order to understand the loss dynamics observed in Fig. 2(b), we have to consider two main effects. The first one is three-body (3B) recombination, which causes strong losses mainly in state 1, where the measured 3B loss rate is $K_{111}/3! = 9 \times 10^{-28} \text{ cm}^6/\text{s}$, with an uncertainty up to a factor of 2 [21]. The second one is related to a stabilization mechanism of the mixture: The droplet forms with a specific population imbalance, $N_1/N_2 = \sqrt{a_{22}/a_{11}}$ [1]. It can bear only a deviation from that value which corresponds to an increase of the atom number in one of the two components $\delta N_i/N_i \sim |\delta a|/a_{ii}$, $i = 1, 2$ [1]. Any excess of atoms beyond this threshold is not bound to the droplet and expands as a gas. Combining these two mechanisms, we can interpret the behavior observed in Figs. 2(b) and 2(c). In the first 2 ms, the ratio N_1/N_2 decreases, meaning that the mixture is mainly losing atoms in state 1, due to the stronger 3B losses in that component. When the mixture reaches the equilibrium population imbalance, the ratio N_1/N_2 stabilizes, meaning that 3B losses in state 1 are accompanied by a release of atoms in state 2 into an unbound fraction. This is also compatible with the bimodal density profiles we observe both in the expansion in Fig. 2(a) and in the Stern-Gerlach measurements in Figs. 2(b) and 2(c). We can indeed distinguish a dense central cloud, corresponding to the droplet, surrounded by low-density tails corresponding to the unbound expanding atoms. We thus fit the profiles with the sum of two Gaussians. The data reported in Fig. 2 correspond to the size and atom numbers of the central part [inset in Fig. 2(a)]. Note that the low-density tails are not visible for short t , so that they cannot be associated to an initial thermal cloud. In the Stern-Gerlach measurements, they are mainly visible in state 2, compatibly with our understanding of the loss dynamics.

In Fig. 2(a), we observe a dynamical evolution of the size also during the droplet phase before t_c . The mixture is indeed prepared out of equilibrium, the initial size being larger than the droplet nominal size. In addition to that, N is decreasing due to losses, so that σ needs to decrease to preserve the droplet equilibrium density [1]. To understand the timescales of this dynamics and verify if what we observe is compatible with the predictions of the model from Ref. [1], we perform a numerical simulation. We integrate numerically a system of two generalized

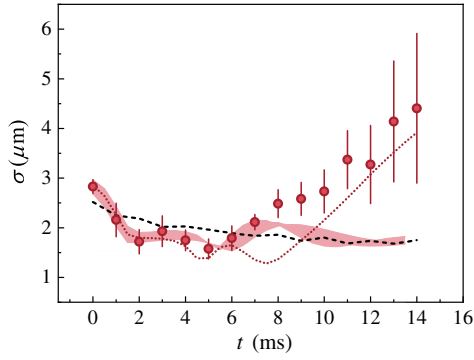


FIG. 3. Evolution of the size σ for $B = 56.54(1)$ G compared with the results of the numerical simulations for $N = 250(50) \times 10^3$, $K_{111}/3! = 9 \times 10^{-28} \text{ cm}^6/\text{s}$ (colored area) and $N = 250 \times 10^3$, $K_{111}/3! = 18 \times 10^{-28} \text{ cm}^6/\text{s}$ (dotted line). The dashed line is the equilibrium size calculated according to Ref. [1] for the measured N in Fig. 2(b).

Gross-Pitaevskii equations, which include first-order quantum corrections in the local chemical potential [9] via the two-species LHY term discussed in Ref. [1] and 3B losses in state 1 [21]. We observe the evolution of the mixture, and we fit the density profiles as in the experiment. As shown in Fig. 3, in the first part of the evolution, up to ~ 8 ms, we find a very good agreement with the data. At larger times, while in the experiment we observe a transition to the gas phase, the mixture is still self-bound in the simulation. A better agreement at large times is obtained by increasing the value of K_{111} to twice its measured value (dotted line), which is still compatible with the error bar in the measurement of the loss rate [21]. We also compare the observed evolution with the equilibrium droplet size predicted in the theory of Ref. [1]. We calculate the droplet radius $R/\sqrt{2}$ defined in Ref. [1] as a function of the measured atom number at each time (dashed line). The behavior of $\sigma(t)$ is thus explained by a contraction of the mixture to its equilibrium size plus an oscillation on top of that. Interestingly, despite the limited lifetime, the contraction dynamics is fast enough to allow us to observe the droplet close to its equilibrium configuration. We can then directly compare our experimental data with the predictions from Ref. [1].

We repeat the measurements of Fig. 2 for different values of B . From the expansions as in Fig. 2(a), we measure the size of the droplet as the average of σ in the observed plateau between the initial contraction and the final expansion [rectangle in Fig. 2(a)] [21]. In Fig. 4(a), we compare our results with the theoretical expectations for σ in the atom number range corresponding to the plateau, i.e., $N_c \lesssim N \lesssim 2N_c$. We also plot the measured aspect ratio σ_x/σ_z , showing that the droplet is isotropic. In Figs. 4(b) and 4(c), we plot the critical atom numbers N_c and ratios N_1/N_2 , measured as the average of N and N_1/N_2 for $t > t_c$. We compare N_c with the predicted values for

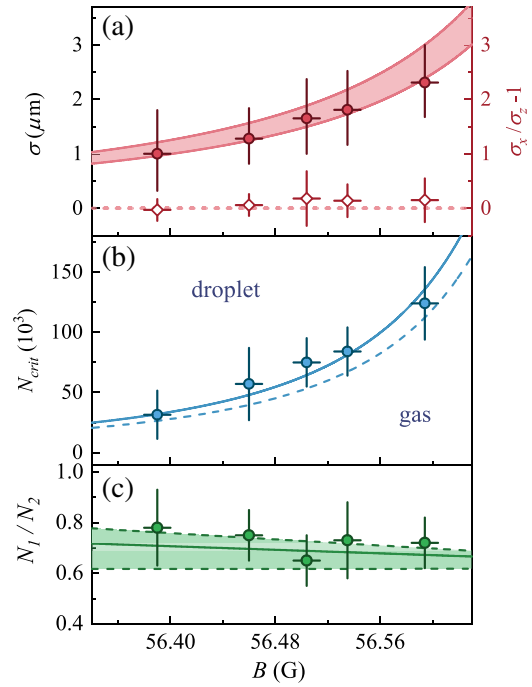


FIG. 4. Measured values of σ (a), N_c (b), and N_1/N_2 (c) as a function of the magnetic field B . In (a), we also report σ_x/σ_z (diamonds). The colored area in (a) corresponds to the theoretical prediction for σ for $N_c \lesssim N \lesssim 2N_c$. The curves in (b) correspond to the predicted critical atom number for the metastable (dashed) and stable (solid) self-bound solutions. In (c), the theoretical curves are obtained as in Fig. 2(c). The vertical error bars correspond to the statistical uncertainty. The horizontal ones are due to the uncertainty in the magnetic field calibration. All error bars correspond to one standard deviation.

the metastable (dashed line) and stable (solid line) self-bound solutions as defined in Ref. [1] [Fig. 4(b)]. In Fig. 4(c), N_1/N_2 is compared with the theoretical value $N_1/N_2 = \sqrt{a_{22}/a_{11}}$, considering also the allowed deviations $\delta N_i/N_i$ introduced above. The agreement of the experimental data with the theory is visibly good for all the measured parameters over the entire magnetic field range we explored.

In conclusion, we have observed self-bound droplets in an atomic Bose-Bose mixture in free space. By measuring the size and the critical atom number as a function of the MF attraction, we have provided a confirmation of the theoretical model in Ref. [1]. The realization of spherical droplets paves the way to studies on their most peculiar property, self-evaporation, with the aim to probe the regime of its occurrence [1] and to characterize how the system dissipates energy by expelling atoms. It will also be interesting to study the droplet in reduced dimensionality [30,31] and its response to a coherent intercomponent coupling [32] or to investigate differences and analogies with other self-bound quantum fluids like helium clusters [33,34], probing the superfluid behavior [35–37] and

comparing the excitation spectra [38]. Finally, our work triggers the possibility to investigate the formation of self-bound droplets in different atomic mixtures, possibly with reduced 3B loss rates and longer lifetimes [39–43].

We acknowledge insightful discussions with D. Petrov, A. Simoni, S. Stringari, A. Recati, L. Tarruell, L. Tanzi, and our colleagues of the Quantum Degenerate Gases group at LENS. We thank G. Spagnolli for assistance in the early stages of the experiment. This work was supported by the ERC Starting Grant AISENS No. 258325 and by EC-H2020 Grant QUIC No. 641122. M. M. acknowledges support by the Spanish Ministry of Economy, Industry, and Competitiveness (MINECO) and the European Regional Development Fund FEDER through Grant No. FIS2015-67161-P (MINECO/FEDER, UE), and the Basque Government through Grant No. IT986-16.

*semeghini@lens.unifi.it

- [1] D. S. Petrov, *Phys. Rev. Lett.* **115**, 155302 (2015).
- [2] E. A. Donley, N. R. Claussen, S. L. Cornish, J. L. Roberts, E. A. Cornell, and C. E. Wieman, *Nature (London)* **412**, 295 (2001).
- [3] T. D. Lee, K. Huang, and C. N. Yang, *Phys. Rev.* **106**, 1135 (1957).
- [4] H. Kadau, M. Schmitt, M. Wenzel, C. Wink, T. Maier, I. Ferrier-Barbut, and T. Pfau, *Nature (London)* **530**, 194 (2016).
- [5] I. Ferrier-Barbut, H. Kadau, M. Schmitt, M. Wenzel, and T. Pfau, *Phys. Rev. Lett.* **116**, 215301 (2016).
- [6] M. Schmitt, M. Wenzel, F. Böttcher, I. Ferrier-Barbut, and T. Pfau, *Nature (London)* **539**, 259 (2016).
- [7] L. Chomaz, S. Baier, D. Petter, M. J. Mark, F. Wächtler, L. Santos, and F. Ferlaino, *Phys. Rev. X* **6**, 041039 (2016).
- [8] I. Ferrier-Barbut, M. Schmitt, M. Wenzel, H. Kadau, and T. Pfau, *J. Phys. B* **49**, 214004 (2016).
- [9] F. Wächtler and L. Santos, *Phys. Rev. A* **93**, 061603(R) (2016).
- [10] D. Baillie, R. M. Wilson, R. N. Bisset, and P. B. Blakie, *Phys. Rev. A* **94**, 021602(R) (2016).
- [11] M. Wenzel, F. Böttcher, T. Langen, I. Ferrier-Barbut, and T. Pfau, *Phys. Rev. A* **96**, 053630 (2017).
- [12] I. Ferrier-Barbut, M. Wenzel, M. Schmitt, F. Böttcher, and T. Pfau, *Phys. Rev. A* **97**, 011604(R) (2018).
- [13] I. Ferrier-Barbut, M. Wenzel, F. Böttcher, T. Langen, M. Isoard, S. Stringari, and T. Pfau, *Phys. Rev. Lett.* **120**, 160402 (2018).
- [14] C. R. Cabrera, L. Tanzi, J. Sanz, B. Naylor, P. Thomas, P. Cheiney, and L. Tarruell, *Science* **359**, 301 (2018).
- [15] P. Cheiney, C. R. Cabrera, J. Sanz, B. Naylor, L. Tanzi, and L. Tarruell, *Phys. Rev. Lett.* **120**, 135301 (2018).
- [16] I. Ferrier-Barbut and T. Pfau, *Science* **359**, 274 (2018).
- [17] D. S. Petrov, *Nat. Phys.* **14**, 211 (2018).
- [18] D. Baillie, R. M. Wilson, and P. B. Blakie, *Phys. Rev. Lett.* **119**, 255302 (2017).
- [19] The scattering lengths are calculated according to the model described in S. Roy, M. Landini, A. Trenkwalder, G. Semeghini, G. Spagnolli, A. Simoni, M. Fattori, M. Inguscio, and G. Modugno, *Phys. Rev. Lett.* **111**, 053202 (2013).
- [20] F. Dalfovo, S. Giorgini, L. P. Pitaevskii, and S. Stringari, *Rev. Mod. Phys.* **71**, 463 (1999).
- [21] See Supplemental Material at <http://link.aps.org/supplemental/10.1103/PhysRevLett.120.235301> for complete sets of measurements and further details about the experimental techniques and theoretical models we used. It includes Refs. [22–28].
- [22] W. Muessel, H. Strobel, M. Joos, E. Nicklas, I. Stroescu, J. Tomkovič, D. B. Hume, and M. K. Oberthaler, *Appl. Phys. B* **113**, 69 (2013).
- [23] M. Zaccanti, B. Deissler, C. D’Errico, M. Fattori, M. Jonas-Lasinio, S. Müller, G. Roati, M. Inguscio, and G. Modugno, *Nat. Phys.* **5**, 586 (2009).
- [24] F. Wächtler and L. Santos, *Phys. Rev. A* **94**, 043618 (2016).
- [25] C. Menotti and S. Stringari, *Phys. Rev. A* **66**, 043610 (2002).
- [26] B. Jackson, J. F. McCann, and C. S. Adams, *J. Phys. B* **31**, 4489 (1998).
- [27] P. A. Altin, G. R. Dennis, G. D. McDonald, D. Döring, J. E. Debs, J. D. Close, C. M. Savage, and N. P. Robins, *Phys. Rev. A* **84**, 033632 (2011).
- [28] J. Schuster, A. Marte, S. Amtage, B. Sang, G. Rempe, and H. C. W. Beijerinck, *Phys. Rev. Lett.* **87**, 170404 (2001).
- [29] V. Cikojević, K. Dželalija, P. Stipanović, and L. Vranješ Markić, and J. Boronat, *Phys. Rev. B* **97**, 140502(R) (2018).
- [30] D. S. Petrov and G. E. Astrakharchik, *Phys. Rev. Lett.* **117**, 100401 (2016).
- [31] D. Edler, C. Mishra, F. Wächtler, R. Nath, S. Sinha, and L. Santos, *Phys. Rev. Lett.* **119**, 050403 (2017).
- [32] A. Cappellaro, T. Macrì, G. F. Bertacco, and L. Salasnich, *Sci. Rep.* **7**, 13358 (2017).
- [33] F. Dalfovo and S. Stringari, *J. Chem. Phys.* **115**, 10078 (2001).
- [34] M. Barranco, R. Guardiola, S. Hernández, R. Mayol, J. Navarro, and M. Pi, *J. Low Temp. Phys.* **142** (2006).
- [35] S. Grebenev, J. P. Toennies, and A. F. Vilesov, *Science* **279**, 2083 (1998).
- [36] L. F. Gomez *et al.*, *Science* **345**, 906 (2014).
- [37] Y. Li, Z. Chen, Z. Luo, C. Huang, H. Tan, W. Pang, and B. A. Malomed, [arXiv:1801.10274](https://arxiv.org/abs/1801.10274).
- [38] M. Casas and S. Stringari, *J. Low Temp. Phys.* **79**, 135 (1990).
- [39] T. A. Schulze, T. Hartmann, K. K. Voges, M. W. Gempel, E. Tiemann, A. Zenesini, and S. Ospelkaus, *Phys. Rev. A* **97**, 023623 (2018).
- [40] G. Modugno, M. Modugno, F. Riboli, G. Roati, and M. Inguscio, *Phys. Rev. Lett.* **89**, 190404 (2002).
- [41] G. Thalhammer, G. Barontini, L. De Sarlo, J. Catani, F. Minardi, and M. Inguscio, *Phys. Rev. Lett.* **100**, 210402 (2008).
- [42] L. Wacker, N. B. Jørgensen, D. Birkmose, R. Horchani, W. Ertmer, C. Klempt, N. Winter, J. Sherson, and J. J. Arlt, *Phys. Rev. A* **92**, 053602 (2015).
- [43] T. Karpiuk, D. Rakshit, M. Brewczyk, and M. Gajda, [arXiv:1801.00346](https://arxiv.org/abs/1801.00346).